RSC Sustainability

ROYAL SOCIETY OF CHEMISTRY

PAPER

View Article Online
View Journal | View Issue

Cite this: *RSC Sustainability*, 2024, **2**, 1568

Co-electrolysis SOEC and internal reforming SOFC for achieving a carbon-neutral society

Hirofumi Sumi *

Solid oxide electrolysis cells (SOECs) can produce carbon monoxide (CO) from carbon dioxide (CO_2) in addition to hydrogen (H_2) from steam using renewable energy sources such as solar and wind power. Methanol (MeOH) and dimethyl ether (DME) are industrially synthesized from syngas (H_2 + CO mixture) with an H_2/CO ratio of 2. Solid oxide fuel cells (SOFCs) can generate power using MeOH and DME in addition to H_2. To achieve a carbon-neutral society, H_2O/CO_2 co-electrolysis SOECs and internal reforming SOFCs using MeOH and DME were investigated using the same negatrode-supported microtubular cells. As a result of quantitative analysis of the gas composition, the H_2/CO ratios of the product gases were identical to the H_2O/CO_2 ratios of the input gases during the co-electrolysis. The gas diffusion resistance increased with decreasing H_2O/CO_2 ratios for co-electrolysis SOECs, and increased with time during co-electrolysis at $H_2O/CO_2 = 2$ and internal reforming of MeOH and DME. H_2O/CO_2 co-electrolysis SOECs and internal reforming SOFCs using MeOH and DME were successfully operated for 100 h.

Received 24th February 2024
Accepted 21st April 2024

DOI: 10.1039/d4su00095a

rsc.li/rscsus

Sustainability spotlight

To achieve a carbon-neutral society, converting carbon dioxide (CO_2) into raw materials and synthetic fuels (e-fuel) is very important. Solid oxide electrolysis cells (SOECs) can produce syngas (H_2 + CO mixture) from steam and CO_2 using renewable energy sources such as solar and wind power. Syngas can be converted into methanol (MeOH) and dimethyl ether (DME) in addition to e-fuel such as gasoline, kerosene, and diesel *via* Fischer–Tropsch synthesis. MeOH and DME are fuels for solid oxide fuel cells (SOFCs) in addition to raw materials for commodity plastics (e-chemical). The reversible SOECs and SOFCs using carbon-containing fuels contribute to the following UN sustainable development goals: affordable and clean energy (SDG 7), responsible consumption and production (SDC 12), and climate action (SDG 13).

1. Introduction

Solid oxide fuel cells (SOFCs) are expected to be power generation systems with high energy conversion efficiencies. SOFCs can directly use hydrocarbon and alcohol fuels in addition to hydrogen (H_2), because oxide ions (O^{2-}) conduct through an electrolyte and the electrochemical oxidation occurs at the negatrode (fuel electrode) at high temperatures above 600 °C.[1–3] Power generation with internal partial oxidation reforming of butane and steam reforming of ethanol has been investigated using microtubular SOFCs supported on a Ni-Gd-doped ceria (GDC) negatrode.[4] A long-term flight of a drone (UAV; unmanned aerial vehicle) was demonstrated using a portable SOFC system powered by liquefied petroleum gas (LPG) cartridges.[5] Because LPG is a fossil fuel, replacing LPG with carbon-neutral fuels is desirable. Although bio-ethanol helps to reduce carbon dioxide (CO_2) emissions, sulfur-containing bio-fuels deteriorate Ni-based SOFC negatrodes by promoting carbon deposition.[6]

Solid oxide cells can be used as electrolyzers as shown in Fig. 1. Solid oxide electrolysis cells (SOECs) can produce carbon monoxide (CO) from CO_2 in addition to H_2 from steam *via* the reverse reaction of SOFCs with O^{2-} conduction through the electrolyte. Alkaline and polymer electrolyte membrane (PEM) electrolysis are widely demonstrated for H_2 production.[7] Some researchers have investigated low-temperature CO_2 electrolysis using alkaline aqueous electrolytes and PEMs. However, these require a high cell voltage above 2.5 V, and these exhibit a low faradaic efficiency.[8] On the contrary, SOECs can produce CO at 1.4 V *via* high-temperature CO_2 electrolysis, resulting in faradaic and energy efficiencies of 100% in principle. If external thermal energy can compensate for the latent heat of water vaporization and endothermic electrolysis, a further decrease in cell voltage and an increase in efficiency are possible.

CO_2 capture is one of the most important technologies for achieving a carbon-neutral society. Chemical adsorption method involving monoethanolamine and gas separation membranes have been demonstrated for CO_2 capture.[9] The initial target is treating the exhaust gases from plants, which

Innovative Functional Materials Research Institute, National Institute of Advanced Industrial Science and Technology (AIST), Nagoya, Aichi 463-8560, Japan. E-mail: h-sumi@aist.go.jp

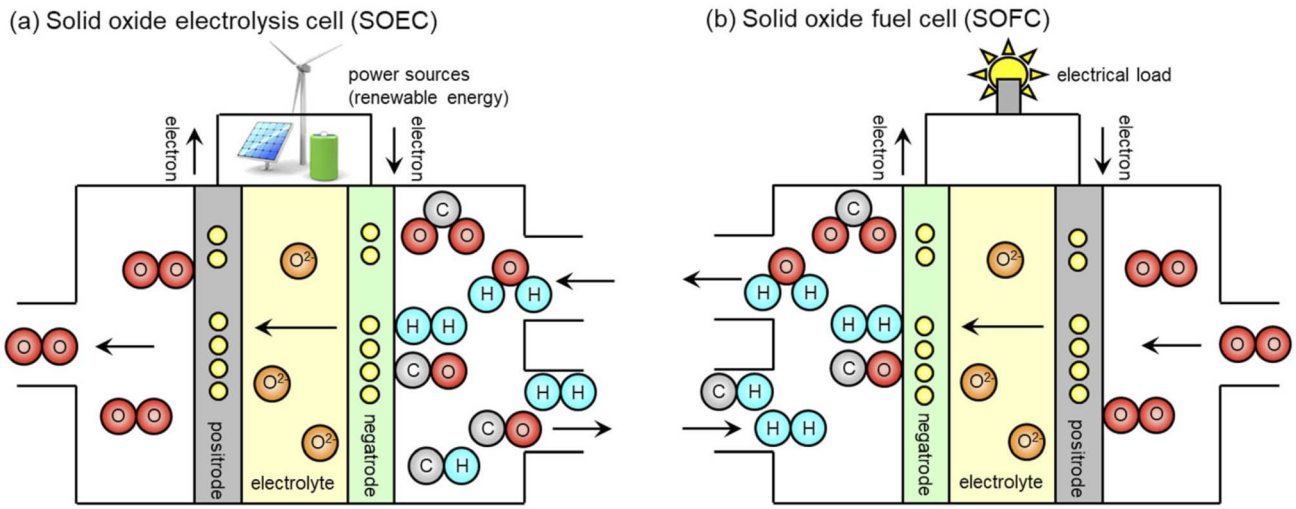

Fig. 1 Schematics of (a) co-electrolysis SOEC and (b) internal reforming SOFC.

contain 4–14 vol% CO_2. Recently, direct air capture (DAC), which extracts CO_2 directly from the atmosphere at any location, has been investigated.[10] Mixed ionic liquid membranes exhibit a high CO_2 permeability of 2.5983×10^{-6} $cm^3(STP)\cdot cm\ cm^{-2}\ s^{-1}\ cm_{Hg}^{-1}$ and a high CO_2/N_2 selectivity of 1.0059×10^4 at 400 ppm CO_2.[11]

SOECs can simultaneously perform steam and CO_2 electrolysis, known as co-electrolysis.[12–16] Syngas, a mixture of H_2 and CO, is produced *via* the co-electrolysis SOECs. Syngas can be converted into many useful sources and fuels as follows:

$$\text{Methanation: } 3H_2 + CO \rightarrow CH_4 + H_2O \quad (1)$$

$$\text{Fischer–Tropsch synthesis: } (2n+1)H_2 + nCO \rightarrow C_nH_{2n+2} + nH_2O \quad (2)$$

$$\text{Methanol synthesis: } 2H_2 + CO \rightarrow CH_3OH \quad (3)$$

$$\text{Dimethyl ether (DME) synthesis: } 4H_2 + 2CO \rightarrow CH_3OCH_3 + H_2O \quad (4)$$

Methanation is used to produce synthetic natural gas,[17] with the advantage of utilizing existing pipelines and infrastructure. However, the SOFCs using synthetic natural gas require a high temperature of 790 °C for methane reforming. Fischer–Tropsch (FT) synthesis is used to produce synthetic fuels (e-fuel) such as gasoline, kerosene, and diesel for airplanes, vessels, and large vehicles.[18] A Co/SiO_2 catalyst yields 1500 and 815 g $kg_{\text{-cat}}^{-1}\ h^{-1}$ of C_{5+} and C_{10-20} hydrocarbons, respectively, *via* FT synthesis at 776 °C and 1.1 MPa.[19] However, SOFCs easily deteriorate because of carbon deposition, when hydrocarbons with high carbon number are used as fuels. Therefore, the author focuses on methanol (MeOH) and dimethyl ether (DME). MeOH is industrially produced from syngas generated by natural gas reforming using Cu/ZnO-based catalysts.[20–22] Direct methanol fuel cells (DMFCs) using PEM electrolyte have been investigated owing to their low reforming temperatures below 150 °C.[23] However, DMFCs suffer from CO poisoning on a negatrode and MeOH crossover through an electrolyte. For SOFCs, MeOH is a promising fuel, because it does not cause CO poisoning and MeOH crossover.[24–27] In addition, DME can be easily produced by the dehydration of methanol.[28]

$$\text{DME synthesis: } 2CH_3OH \rightarrow CH_3OCH_3 + H_2O \quad (5)$$

The reforming temperature of DME is less than 180 °C, and its characteristics are similar to those of LPG, because it is easily liquified at 0.6 MPa. Thus, DME is a possible alternative to LPG as a fuel for portable SOFC systems.[29,30]

In the present work, co-electrolysis SOECs and internal reforming SOFCs were investigated using microtubular negatrode-supported cells with the same cell configuration. Numerous researchers have demonstrated reversible SOFC/SOEC operation using H_2 and steam.[31–33] However, there have been few demonstrations of reversible operation using carbon-containing fuels. The H_2/CO ratio of the syngas should be 2 for MeOH, DME, and FT syntheses. To investigate the effect of CO_2 concentration on electrochemical characteristics, co-electrolysis was performed with varying H_2O/CO_2 ratios from 0 to infinity (∞). The compositions of the product gases after co-electrolysis were analyzed using gas chromatography. Assuming that MeOH and DME are synthesized from syngas, internal reforming SOFCs were demonstrated using MeOH and DME. Steam reforming was investigated for MeOH, because it is a liquid with water solubility. Partial oxidation reforming was investigated for DME in addition to steam reforming, since it easily mixes with ambient air at ordinary temperatures and pressures. Short-term durability tests of the co-electrolysis SOECs using an input gas at $H_2O/CO_2 = 2$ and internal reforming SOFCs using MeOH and DME were conducted for 100 h.

2. Experimental

2.1 Cell preparation

Similar to previously reported internal reforming of butane and ethanol,[4] negatrode-supported microtubular cells with the same

cell configuration were used for co-electrolysis SOECs and internal reforming SOFCs using MeOH and DME. Negatrode microtube substrates were constructed using 60 wt% NiO (Sumitomo Metal Mining)-40 wt% $Ce_{0.9}Gd_{0.1}O_{1.95}$ (GDC; Shin-Etsu Chemical) adding pore former (acrylic resin; Sekisui Plastic) and binder (cellulose; Yuken Kogyo) powders. These powders were mixed using a kneading machine with adding an appropriate amount of water, and the negatrode microtubes were extruded using a piston cylinder. After extrusion, the microtubes were dried overnight in air at room temperature. A slurry was prepared by mixing $(Y_2O_3)_{0.08}(ZrO_2)_{0.92}$ (YSZ; Tosoh), binder (polyvinyl butyral; Sekisui Chemical) dispersant (tallow propylene diamine, Kao Chemicals) and plasticizer (dioctyl adipate; Wako Pure Chemical Industries) with ethanol and toluene solvents. The YSZ electrolyte was formed by dip-coating. The YSZ electrolyte thin-film and the NiO–GDC negatrode microtube were co-sintered in air for 3 h at 1400 °C. The GDC interlayer and the positrode (air electrode) of 70 wt% $La_{0.6}Sr_{0.4}Co_{0.2}Fe_{0.8}O_{3-\delta}$ (LSCF; Kusaka Rare Metal)-30 wt% GDC were coated in a similar manner. The interlayer and positrode thin-film layers were sintered sequentially in air for 2 h at 1200 °C and for 1 h at 1050 °C, respectively. The microtube diameter and positrode area after sintering were 2.8 mm and 2.6 cm^2, respectively. The thicknesses of the negatrode, electrolyte, interlayer, and positrode were 640, 10, 1, and 20 μm, respectively.

2.2 Evaluation of co-electrolysis SOECs and internal reforming SOFCs

Table 1 and Fig. 2 show the experimental conditions and setup for evaluating the co-electrolysis SOECs and internal reforming SOFCs. For internal steam reforming of MeOH, an aqueous MeOH solution (82 vol% at S/C = 0.5 and 69 vol% at S/C = 1.0) was supplied to the negatrode using a pump and vaporizer heated at 250 °C. For co-electrolysis and internal steam reforming of DME, steam was fed to the negatrode using a temperature-controlled bubbler. Before evaluation, a mixture of 20% H_2-3% H_2O-77% N_2 was supplied to the negatrode for 2 h at 700 °C for Ni catalyst reduction. Subsequently, the input gases were adjusted to the flow rates listed in Table 1, and air was supplied to the positrode at a rate of 100 mL min^{-1}. Hydrogen was supplied during co-electrolysis SOEC to prevent Ni catalyst oxidation in the negatrode under open circuit voltage (OCV). Current–voltage (*I–V*) characteristics were evaluated using a potentiostat/galvanostat (Solartron Analytical 1470E) by varying the voltage from OCV to 0.4 and 1.4 V for SOECs and SOFCs, respectively, at a sweep rate of 5 mV s^{-1}. Using a frequency response analyzer (Solartron Analytical 1455), the electrochemical impedance between the negatrode and positrode was measured in the frequency range of 100 kHz–0.1 Hz with 20 steps per logarithmic decade. The polarization impedance can be deconvoluted using the distribution of relaxation times (DRT) analysis.[34,35] The DRT analysis was performed using

Table 1 Flow rates (mL min^{-1}) of the input gases for co-electrolysis SOECs and internal steam (SR) and partial oxidation (POx) reforming SOFCs

	H_2O/CO_2	H_2	H_2O	CO_2	O_2	MeOH or DME	N_2
Co-electrolysis	$H_2O/CO_2 = 0$	3.0	0.0	20.0			77.0
	$H_2O/CO_2 = 1/3$	3.0	5.0	15.0			77.0
	$H_2O/CO_2 = 1$	3.0	10.0	10.0			77.0
	$H_2O/CO_2 = 2$	3.0	13.3	6.7			77.0
	$H_2O/CO_2 = 3$	3.0	15.0	5.0			77.0
	$H_2O/CO_2 = \infty$	3.0	20.0	0.0			77.0
MeOH SR	S/C = 0.5		5.0			10.0	85.0
	S/C = 1.0		10.0			10.0	80.0
DME SR	S/C = 1.0		10.0			5.0	85.0
	S/C = 1.5		15.0			5.0	80.0
DME POx	O/C = 1.0				10.0	10.0	61.4
	O/C = 1.5				15.0	10.0	56.4

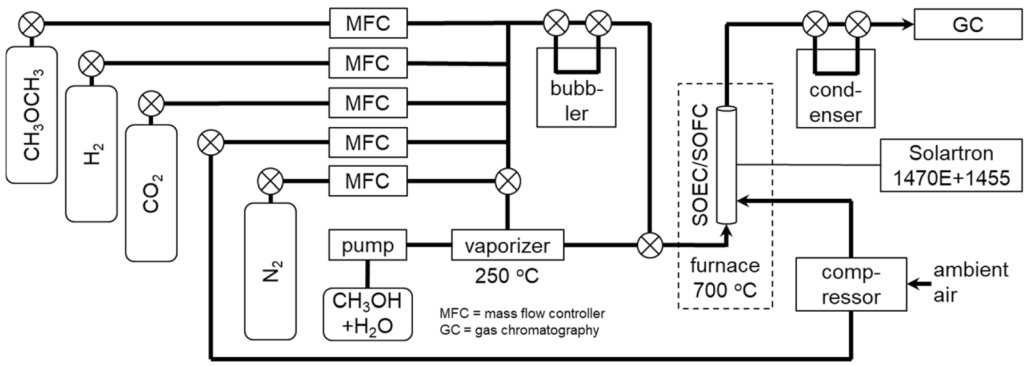

Fig. 2 Schematic of experimental setup for evaluation of co-electrolysis SOECs and internal reforming SOFCs.

Z-Assist software (Toyo Corp.).[36] It used FTIKREG software[37] to solve an ill-posed inverse problem in the DRT analysis *via* Tikhonov regularization. Real impedance was used for the DRT analysis because the impact of measurement errors and inductive components was lower than that with imaginary impedance.[38] Kramers–Kronig validation was performed using K–K test[39] and Lin-KK Tool[40] software. Residuals between measured and Kramers–Kronig transformed impedances were within 0.5%. The parameters obtained DRT analysis were refined by complex non-linear least squares (CNLS) fitting using ZView software (Scribner Associates), assuming an equivalent circuit model with a series connection of resistance (R_0) and parallel resistance-capacitance (R_kC_k) elements. The thermodynamic equilibrium compositions were calculated using HSC Chemistry 5.11 (Outokumpu). During co-electrolysis, the flow rates of the product gases were analyzed with a thermal conductivity detector (TCD) in a micro gas chromatograph (Agilent Technologies 490; Molsieve 5A column with Ar as the carrier gas for H_2, N_2, CH_4, and CO, and PoraPLOT Q column with He as the carrier gas for CO_2). Steam flow rates in the product gases were not measured by micro gas chromatography, because steam was removed using a condenser as shown in Fig. 2. The steam flow rates of the product gases were estimated by considering the mass balance of the hydrogen, oxygen and carbon species. Unfortunately, the flow rates of the reformate gases during internal reforming could not be analyzed, because MeOH and DME are soluble in water. Short-term durability tests of co-electrolysis SOECs and internal reforming SOFCs were conducted for 100 h at a constant voltage of 1.28 V and a constant current density of 0.3 A cm^{-2}, respectively.

3. Results and discussion

3.1 Co-electrolysis SOECs

Fig. 3 shows the equilibrium amounts of the product gases as a function of $H_2O + CO_2$ utilization at (a) $H_2O/CO_2 = 0$ and (b) $H_2O/CO_2 = 2$ at 700 °C. The input gases are 0.2 mol of H_2O/CO_2 and 0.03 mol of H_2. The product amounts of the H_2/CO mixtures are assumed to obey faradaic law. At $H_2O/CO_2 = 0$, carbon is deposited, when $H_2O + CO_2$ utilization exceeds 0.8. At low temperatures, carbon is easily deposited, even at lower H_2O/CO_2 ratios. Moreover, methane is slightly produced, when $H_2O + CO_2$ utilization is above 0.6 at $H_2O/CO_2 = 2$. When carbon and/or methane are not produced, the amounts of H_2 and CO produced increase linearly with the $H_2O + CO_2$ utilization, and the H_2/CO ratios of the product gases are identical to the H_2O/CO_2 ratios of the input gases. Co-electrolysis is desirable to be operated at high temperatures to prevent carbon and methane production.

Fig. 4 shows the *I–V* characteristics for co-electrolysis SOEC at various H_2O/CO_2 ratios and 700 °C. The flow rates of the input gases are listed in Table 1. The theoretical electromotive forces (EMFs) are 0.910, 0.906, 0.902, 0.899, 0.898, and 0.894 V at $H_2O/CO_2 = 0$, 1/3, 1, 2, 3, and ∞, respectively. The OCVs were 20–30 mV lower than the theoretical EMFs under all conditions, owing to slight gas leakage. The slopes of *I–V* curves increased with decreasing H_2O/CO_2 ratios. The $H_2O + CO_2$ utilizations were 0.27–0.32 under 1.28 V at $H_2O/CO_2 = 0 - \infty$. The performances during H_2O/CO_2 co-electrolysis and CO_2 electrolysis

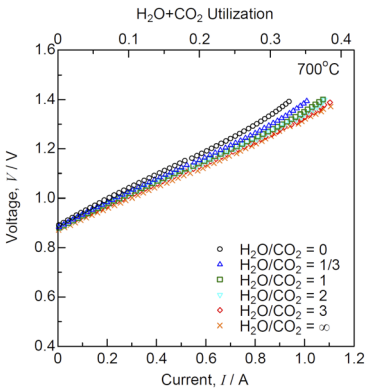

Fig. 4 Current–voltage characteristics for co-electrolysis SOEC at various H_2O/CO_2 ratios and 700 °C.

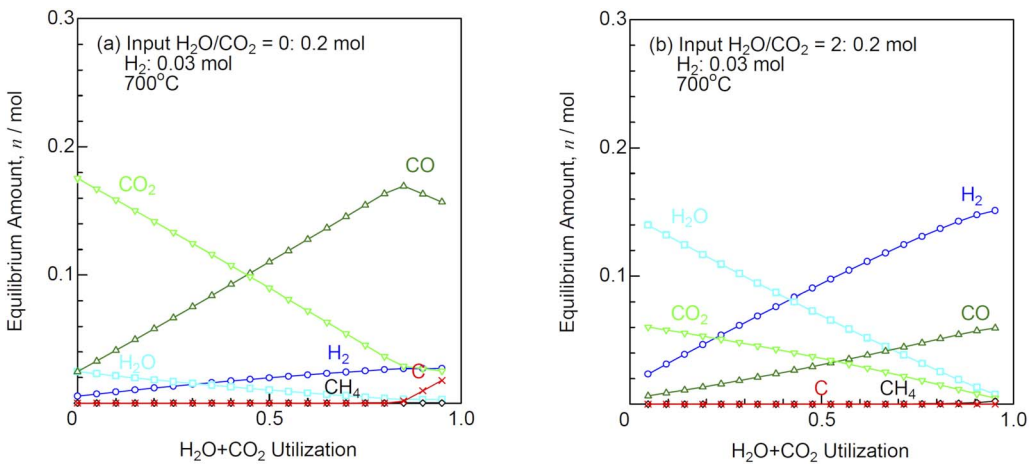

Fig. 3 Equilibrium amounts of the product gases as a function of $H_2O + CO_2$ utilization at (a) $H_2O/CO_2 = 0$ and (b) $H_2O/CO_2 = 2$ (input H_2O/CO_2: 0.2 mol, H_2: 0.03 mol) at 700 °C.

were lower than that during steam electrolysis.[12,13,15,16] The performance of the co-electrolysis SOEC decreased with increasing CO_2 concentrations in the input gases.

Fig. 5(a) and (b) show the Nyquist plots of impedance spectra for co-electrolysis SOEC under OCV and 1.28 V, respectively, at various H_2O/CO_2 ratios and 700 °C. The ohmic losses (R_0) derived from the intersections of the impedance arcs at high frequencies with the real axis remained unchanged with the H_2O/CO_2 ratios. The ohmic losses under 1.28 V were slightly larger than those under OCV, because endothermic reaction of H_2O/CO_2 co-electrolysis decreased the local temperature at the interface between electrolyte and electrode. The polarization resistances at low frequencies below 10 Hz increased with decreasing H_2O/CO_2 ratios. DRT analysis was performed to deconvolute the impedance spectra as shown in Fig. 5(c) and (d). Six DRT peaks were observed under all the conditions, corresponding to the following physicochemical origins of the rate-determining elementary processes for negatrode-supported microtubular SOECs:[36]

P_1 (10–100 kHz): physical impedance originating from the grain boundaries, pores, and reaction products between the electrolyte and positrode

P_2, P_3 (20 Hz–10 kHz): charge transfer and ionic conduction processes at the negatrode

P_4 (2–200 Hz): oxygen surface exchange and diffusion processes at the positrode

P_5, P_6 (0.1–20 Hz): gas diffusion and nonstoichiometric oxygen variation processes at the Ni-GDC negatrode

Fig. 5(e) and (f) show the resistance against H_2O/CO_2 ratios derived from the CNLS fitting using the equivalent circuit model with a series connection of R_0 and six R_kC_k (k = 1–6) elements. R_5 and R_6 increased with decreasing H_2O/CO_2 ratios. Graves *et al.*[12] reported that the polarization resistance resulting from gas diffusion process at the negatrode increased at high CO_2 concentrations. This suggests that the CO/CO_2 mixture diffuses more difficultly than the H_2/H_2O mixture in the SOEC negatrode.

Syngas with an H_2/CO ratio of 2 is desirable for methanol, DME, and FT syntheses. Therefore, a quantitative analysis of product gas compositions is important for the co-electrolysis SOEC evaluation. Table 2 shows the estimated flow rates of the product gases for co-electrolysis SOEC under equilibrium, OCV and 1.28 V using gas chromatography. The steam flow rates were estimated in consideration for mass balance of hydrogen, oxygen and carbon species assuming no carbon deposition. The faradaic law for electrolysis is as follows:

$$I = \dot{n}zF \tag{6}$$

where I is the current (A), $\dot{n}$ is the molar product rate (mol s^{-1}), z is the valency of the ions (2), and F is the faradaic constant (96 485C mol^{-1}). The ideal gas law is as follows:

$$p\dot{v} = 60\dot{n}R_gT \tag{7}$$

Table 2 Estimated flow rates (mL min^{-1}) of the product gases for co-electrolysis SOEC under equilibrium, OCV, and 1.28 V using gas chromatography. The steam flow rates of the product gases were estimated in consideration for mass balance of hydrogen, oxygen and carbon species

H_2O/CO_2	V	I	H_2	H_2O	CO	CO_2	CH_4	N_2
0	Equilibrium		0.543	2.46	2.46	17.5	1×10^{-6}	77.0
	OCV	0 A	0.947	1.65	2.72	17.7	0	77.0
	1.28 V	0.770 A	1.12	2.43	7.70	11.7	0	77.0
1/3	Equilibrium		1.33	6.68	1.68	13.3	5×10^{-6}	77.0
	OCV	0 A	1.58	6.74	1.21	13.5	0	77.0
	1.28 V	0.830 A	3.13	5.33	5.51	9.03	0	77.0
1	Equilibrium		1.98	11.0	1.02	8.98	6×10^{-6}	77.0
	OCV	0 A	1.86	10.7	0.720	9.70	0	77.0
	1.28 V	0.871 A	4.96	7.61	3.80	6.63	0	77.0
2	Equilibrium		2.35	14.0	0.647	6.05	5×10^{-6}	77.0
	OCV	0 A	2.13	13.4	0.538	6.91	0	77.0
	1.28 V	0.886 A	6.22	10.0	2.44	4.31	0	77.0
3	Equilibrium		2.53	15.5	0.469	4.53	4×10^{-6}	77.0
	OCV	0 A	2.38	15.3	0.394	4.95	0	77.0
	1.28 V	0.902 A	7.22	10.6	1.84	3.39	0	77.0
∞	Equilibrium		3.00	20.0	0	0	0	77.0
	OCV	0 A	3.08	19.9	0	0	0	77.0
	1.28 V	0.909 A	9.46	13.5	0	0	0	77.0

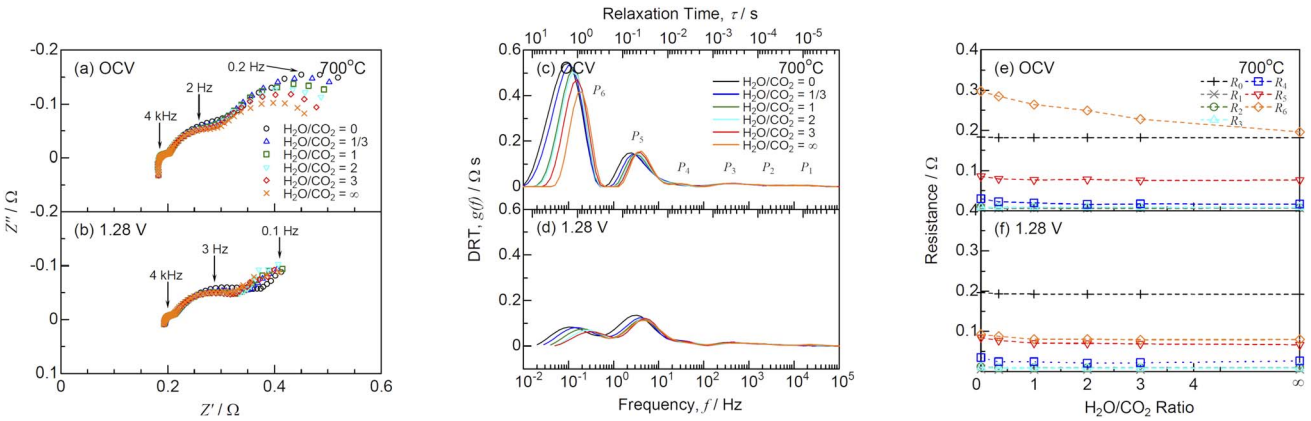

Fig. 5 (a and b) Impedance, (c and d) DRT spectra, and (e and f) resistances for co-electrolysis SOEC under (a, c and e) OCV and (b, d and f)1.28 V at various H_2O/CO_2 ratios and 700 °C.

where p is the pressure (kPa), $\dot{v}$ is the flow rate of the product gas (L min^{-1}), R_g is the gas constant (8.3145 J mol^{-1} K^{-1}), and T is the absolute temperature (K). In the standard state ($p = 101.325$ kPa and $T = 273.15$ K), $\dot{v}$ is derived from the following equation:

$$\dot{v} = 6.9652 \times 10^{-3} I \quad (8)$$

This indicates the production of approximately 7 mL min^{-1} of syngas per 1 A current. Under OCV, the equilibrium compositions differed from the input gas compositions owing to the reverse water gas shift reaction.

$$H_2 + CO_2 \leftrightarrow H_2O + CO \quad (9)$$

The differences between the equilibrium and measured gas flow rates were less than 1 mL min^{-1} under OCV. Under 1.28 V, the H_2 + CO flow rates in the range of 5.15–6.38 mL min^{-1} increased, when the current was 0.770–0.909 A at H_2O/CO_2 = 0 − ∞. The faradaic efficiencies were 0.96–1, because carbon and methane were not produced in the H_2O + CO_2 utilizations ranges of 0.27–0.32. Fig. 6 shows the evolution rates of the product gases for co-electrolysis SOEC at various H_2O/CO_2 ratios and 700 °C. The H_2/CO ratios of the product gases were almost the identical to the H_2O/CO_2 ratios of the input gases. CO_2 electrolysis was slightly more difficult than steam electrolysis, because the polarization resistances increased with decreasing H_2O/CO_2 ratios as shown in Fig. 5. However, CO was produced *via* the reverse water gas shift reaction (eqn (9)) in addition to co-electrolysis. Thus, the product gas compositions easily reached equilibrium compositions.

The short-term durability test was performed under a constant voltage of 1.28 V at $H_2O/CO_2 = 2$ and 700 °C as shown in Fig. 7. Under 1.28 V, the initial current was 0.886 A, which decreased to 0.756 A after 100 h. The slope of the *I*–*V* curves increased, although the OCV remained unchanged during the durability test for 100 h. Fig. 8 shows the (a) impedance, (b) DRT spectra, and (c) resistances for co-electrolysis SOEC during the durability test under a constant voltage of 1.28 V at $H_2O/CO_2 = 2$ and 700 °C. The ohmic loss remained unchanged, whereas the polarization resistances at low frequencies below 10 Hz increased after 100 h. The DRT analysis suggested that R_5 and R_6 related to the gas diffusion process at the negatrode increased with time. The gas diffusion resistance should be decreased to improve durability in addition to the initial performance for co-electrolysis SOECs. Fig. 9 shows the evolution rates of the product gases during the durability test of the co-electrolysis SOEC under a constant voltage of 1.28 V at $H_2O/CO_2 = 2$ and 700 °C. The evolution rates of H_2 and CO decreased with time, because the current decreased from 0.886 A to 0.756 A under 1.28 V after 100 h. The faradaic efficiency was remained above 0.95, confirming that the co-electrolysis SOEC produced syngas with a constant H_2/CO ratio of 2. MeOH and DME syntheses from syngas have been industrially established. Internal reforming SOFCs using MeOH and DME are discussed in the next section.

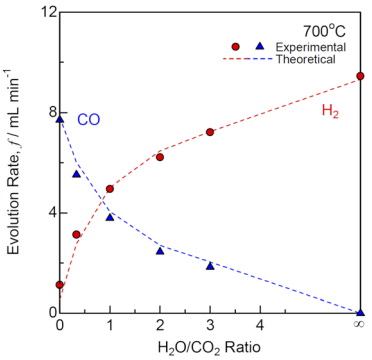

Fig. 6 Evolution rates of the product gases for co-electrolysis SOEC at various H_2O/CO_2 ratios and 700 °C.

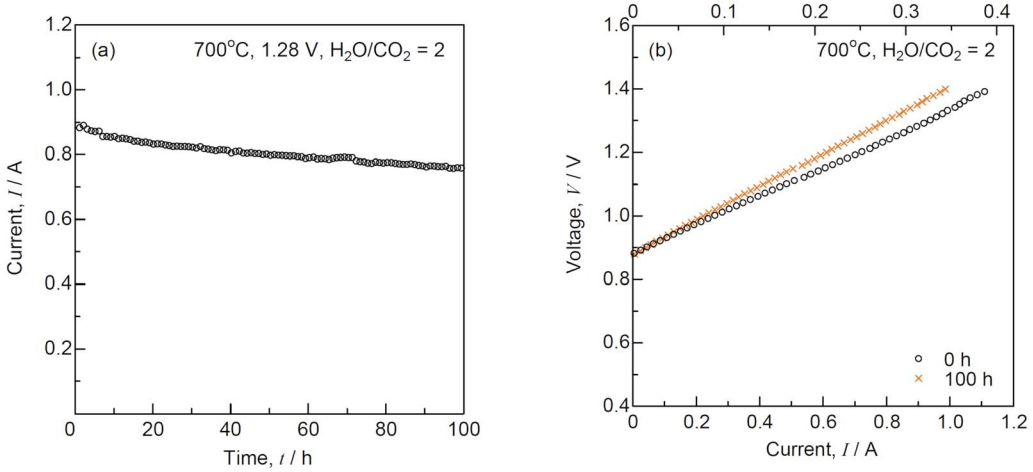

Fig. 7 (a) Time course of current under a constant voltage of 1.28 V and (b) current–voltage characteristics for co-electrolysis SOEC before and after the durability test at $H_2O/CO_2 = 2$ and 700 °C.

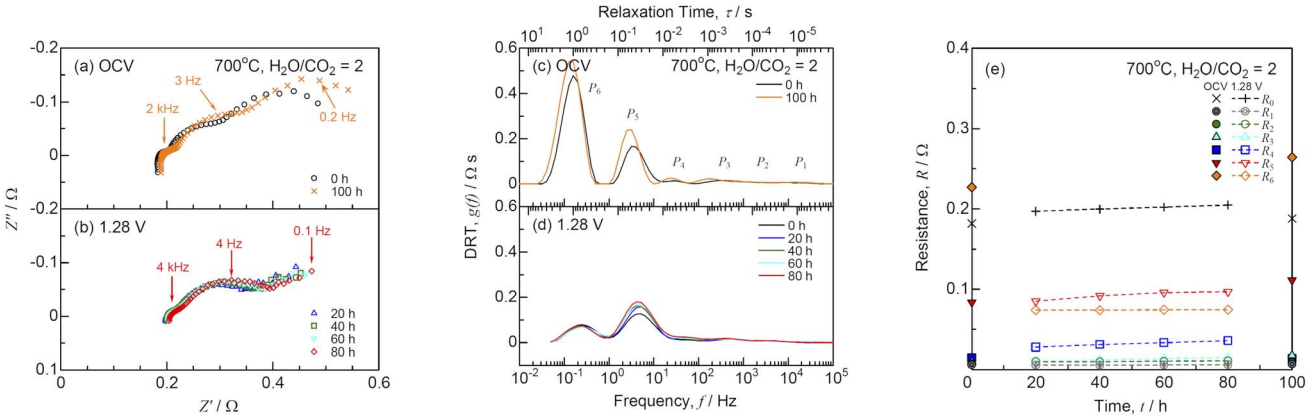

Fig. 8 (a and b) Impedance, (c and d) DRT spectra, and (e) resistances for co-electrolysis SOEC during the durability test under a constant voltage of 1.28 V at $H_2O/CO_2 = 2$ and 700 °C.

3.2 Internal reforming SOFCs

MeOH and DME are easily reformed at low temperatures. The conversion of MeOH and DME reaches 99% at 150 and 180 °C, respectively, in thermodynamic equilibrium. The stoichiometric reaction for MeOH decomposition is as follows:

$$CH_3OH \rightarrow 2H_2 + CO\ \Delta H_{25\ ^\circ C} = +90.5\ kJ\ mol^{-1} \quad (10)$$

Fig. 10(a) shows the equilibrium amounts of the reformate gases as a function of S/C ratio during steam reforming of MeOH at 700 °C. Steam is not required stoichiometrically for MeOH decomposition as shown in eqn (10). However, steam reforming is required to prevent carbon deposition, because carbon is deposited at S/C ratios below 0.3 in equilibrium. Internal reforming SOFCs can be easily supplied with 82 vol% (S/C = 0.5) or 69 vol% (S/C = 1.0) MeOH water solutions. Meanwhile, DME can be reformed using partial oxidation (eqn (12)) in addition to steam (eqn (11)).

$$CH_3OCH_3 + H_2O \rightarrow 4H_2 + 2CO\ \Delta H_{25\ ^\circ C} = +205\ kJ\ mol^{-1} \quad (11)$$

$$CH_3OCH_3 + \tfrac{1}{2}O_2 \rightarrow 3H_2 + 2CO\ \Delta H_{25\ ^\circ C} = -37.0\ kJ\ mol^{-1} \quad (12)$$

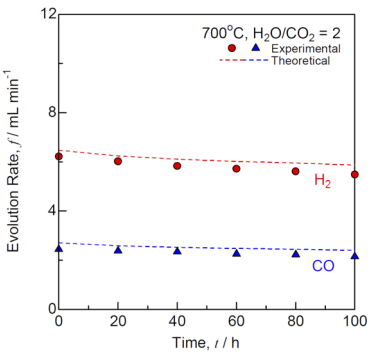

Fig. 9 Evolution rates of the product gases during the durability test of co-electrolysis SOEC under a constant voltage of 1.28 V at $H_2O/CO_2 = 2$ and 700 °C.

Fig. 10(b) and (c) show the equilibrium amounts of the reformate gases as a function of S/C and O/C ratios during steam reforming and partial oxidation reforming of DME at 700 °C. The stoichiometric S/C and O/C ratios are 0.5 for steam reforming and partial oxidation reforming of DME. However,

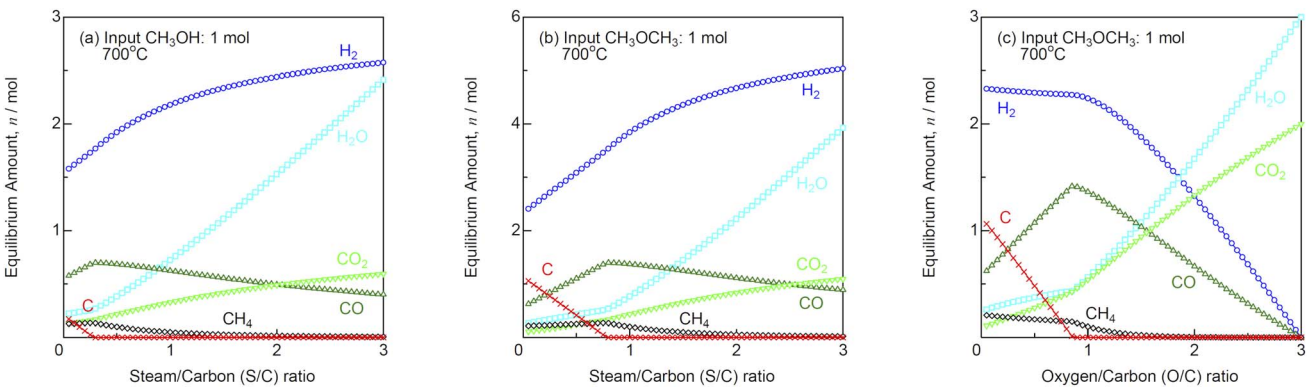

Fig. 10 Equilibrium amounts of the reformate gases as a function of S/C and O/C ratios for (a) steam reforming of MeOH, (b) steam reforming of DME, and (c) partial oxidation reforming of DME (input MeOH or DME: 1 mol) at 700 °C.

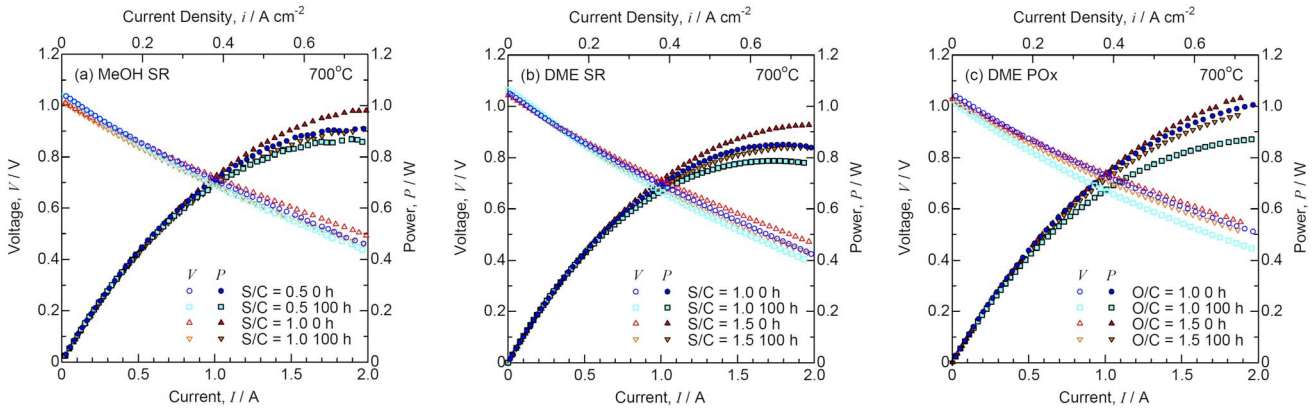

Fig. 11 Current–voltage characteristics for SOFCs during (a) steam reforming (SR) of MeOH, (b) SR of DME, and (c) partial oxidation reforming (POx) of DME before and after the durability tests at 700 °C.

carbon is deposited at S/C ratios <0.8 and O/C ratios <0.9 in equilibrium. The gas characteristics of DME are similar to those of LPG. Therefore, partial oxidation reforming can be easily performed by supplying DME/air mixture.

Fig. 11 shows the *I–V* characteristics for SOFCs during (a) steam reforming of MeOH, (b) steam reforming of DME, and (c) partial oxidation of DME before and after the durability tests at 700 °C. The theoretical EMFs, OCVs, and voltages at 0.3 A cm^{-2} are summarized in Table 3. Unfortunately, the flow rate of the reformate gases during internal reforming could not be determined using the setup as shown in Fig. 2, because water-soluble MeOH and DME were removed from the condenser. The OCVs were almost identical to the theoretical EMFs under all the conditions, suggesting that MeOH and DME were reformed into H_2 and CO by steam and partial oxidation. The OCVs remained unchanged during the durability tests. The *I–V* characteristics were similar during internal reforming of MeOH and DME. Fig. 12 shows the time course of voltage for SOFCs during (a) steam reforming of MeOH, (b) steam reforming of DME, and (c) partial oxidation of DME during the durability test at a constant current density of 0.3 A cm^{-2} and 700 °C. Internal reforming SOFCs using MeOH and DME were continuously operated for 100 h. The degradation rates at different S/C ratios were almost the same during steam reforming of MeOH and DME, whereas the degradation rate at O/C = 1.0 was larger than that at O/C = 1.5 during partial oxidation reforming of DME. Previously, the voltage rapidly dropped during internal reforming of butane at O/C ≤1.0 and ethanol at S/C ≤1.5,[4] although Ni-ceria based negatrodes exhibit high tolerance against carbon deposition.[3,24] The voltage was stable during internal reforming of MeOH and DME, and no carbon deposition was detected at the Ni-GDC negatrode after the durability test. MeOH and DME contain C–O bonds but no C–C bonds, making carbon deposition difficult.[25]

The impedance spectra before and after the durability tests at 700 °C are shown in Fig. 13. Table 3 lists the ohmic losses (R_0) and total polarization resistances (R_p) before and after 100 h. The R_0 values almost remained unchanged during the durability test, whereas those of R_p increased with time. The DRT analysis was performed to deconvolute the impedance spectra as shown in Fig. 14. Four DRT peaks corresponding to P_2–P_5 were detected under all the conditions. Fig. 15 shows the time course of the resistances derived from CNLS fitting using the equivalent circuit model with a series connection of R_0 and four R_kC_k (k = 2–5) elements. The values of R_3 and R_5, which were ascribed to charge transfer and ionic conduction processes, and gas diffusion processes in the negatrode, respectively, increased with time. The DRT peaks of P_3 and P_5 shifted to lower frequencies as shown in Fig. 14. The gas diffusion resistance of the negatrode-supported microtubular cells used in this work

Table 3 Theoretical EMFs, OCVs, voltages at 0.3 A cm^{-2}, ohmic losses and total polarization resistances under OCV for SOFCs during steam reforming (SR) of MeOH, SR of DME, and partial oxidation reforming (POx) of DME before and after the durability test at a constant current density of 0.3 A cm^{-2} and 700 °C

	MeOH SR		DME SR		DME POx	
Ratio	S/C = 0.5	S/C = 1.0	S/C = 1.0	S/C = 1.5	O/C = 1.0	O/C = 1.5
Theoretical EMF	1.04 V	1.02 V	1.04 V	1.02 V	1.03 V	0.997 V
OCV	1.05 V	1.02 V	1.05 V	1.04 V	1.05 V	1.03 V
$V_{0\ h}$@0.3 A cm^{-2}	0.764 V	0.772 V	0.758 V	0.754 V	0.777 V	0.780 V
$V_{100\ h}$@0.3 A cm^{-2}	0.749 V	0.748 V	0.734 V	0.733 V	0.730 V	0.761 V
$R_{0,0\ h}$	0.182 Ω	0.160 Ω	0.200 Ω	0.180 Ω	0.184 Ω	0.165 Ω
$R_{0,100\ h}$	0.182 Ω	0.166 Ω	0.202 Ω	0.179 Ω	0.186 Ω	0.163 Ω
$R_{p,0\ h}$	0.114 Ω	0.115 Ω	0.114 Ω	0.121 Ω	0.122 Ω	0.115 Ω
$R_{p,100\ h}$	0.137 Ω	0.145 Ω	0.151 Ω	0.154 Ω	0.162 Ω	0.145 Ω

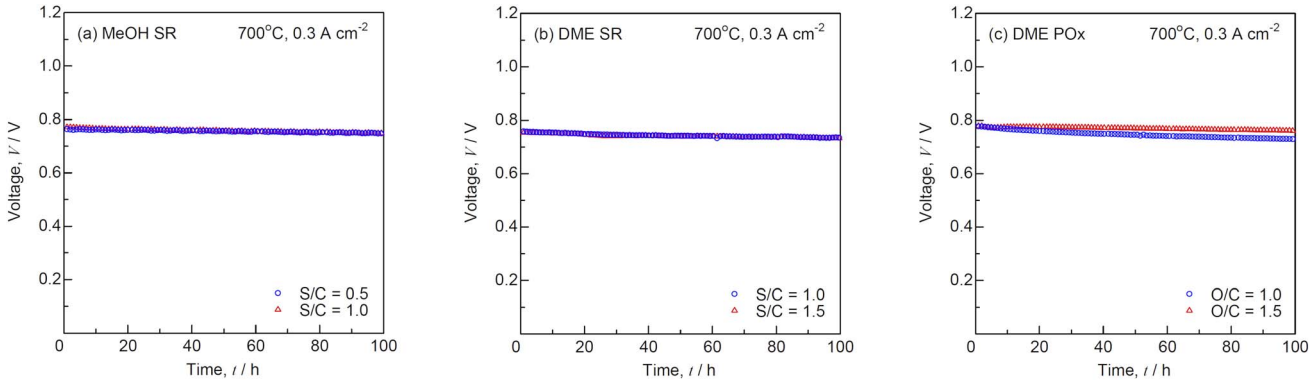

Fig. 12 Time courses of voltage for SOFCs during (a) steam reforming (SR) of MeOH, (b) SR of DME, and (c) partial oxidation reforming (POx) of DME during the durability test at a constant current density of 0.3 A cm^{-2} and 700 °C.

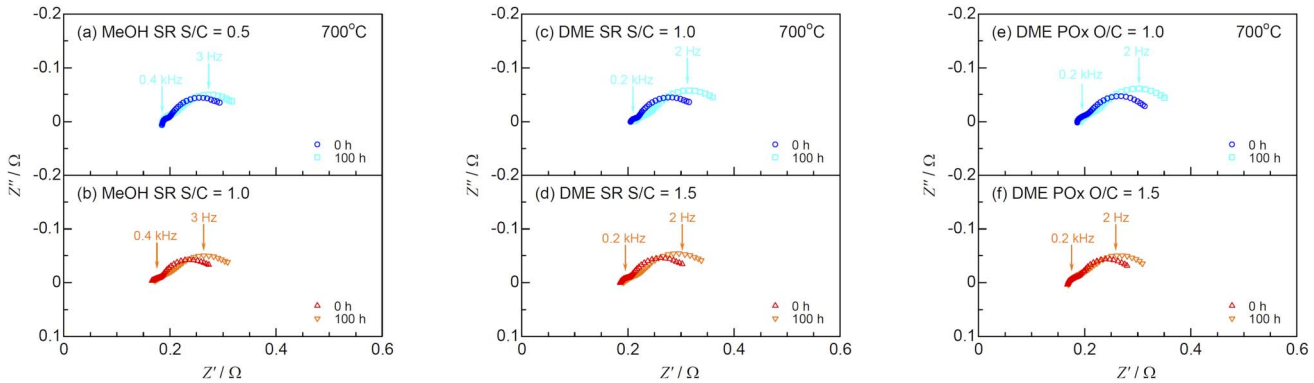

Fig. 13 Impedance spectra for SOFCs during (a and b) steam reforming (SR) of MeOH, (c and d) SR of DME, and (e and f) partial oxidation reforming (POx) of DME before and after the durability tests at 700 °C.

was large, degrading the negatrode performance in charge transfer and gas diffusion processes during internal reforming of MeOH and DME. Thus, optimizing the negatrode microstructure is important for improving the initial performance and durability of co-electrolysis SOECs and internal reforming SOFCs.

3.3 Carbon-neutral energy system using co-electrolysis SOECs and internal reforming SOFCs

Fig. 16 shows a schematic of the carbon-neutral energy system using co-electrolysis SOECs and internal reforming SOFCs. CO_2 is captured from the exhaust gas of plants and directly from the air (DAC).[9–11] Renewable energy sources such as solar and wind

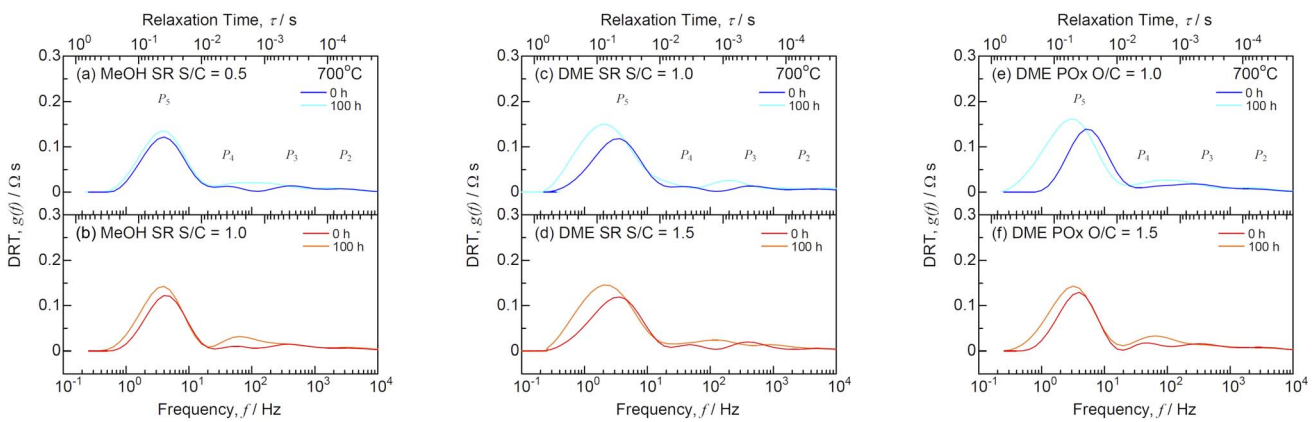

Fig. 14 DRT spectra for SOFCs with (a and b) steam reforming (SR) of MeOH, (c and d) SR of DME, and (e and f) partial oxidation reforming (POx) of DME before and after the durability tests at 700 °C.

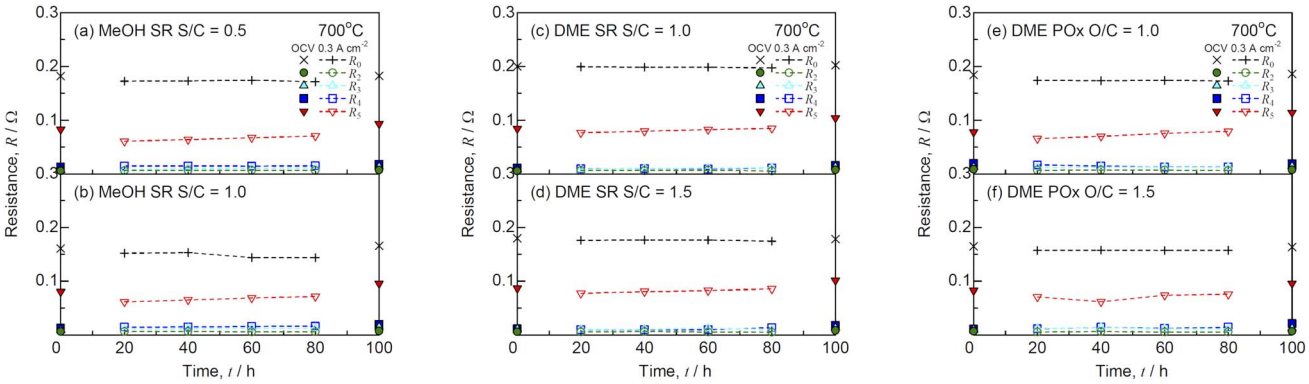

Fig. 15 Time courses of resistances for SOFCs with (a and b) steam reforming (SR) of MeOH, (c and d) SR of DME, and (e and f) partial oxidation reforming (POx) of DME during the durability test at a constant current density of 0.3 A cm^{-2} and 700 °C.

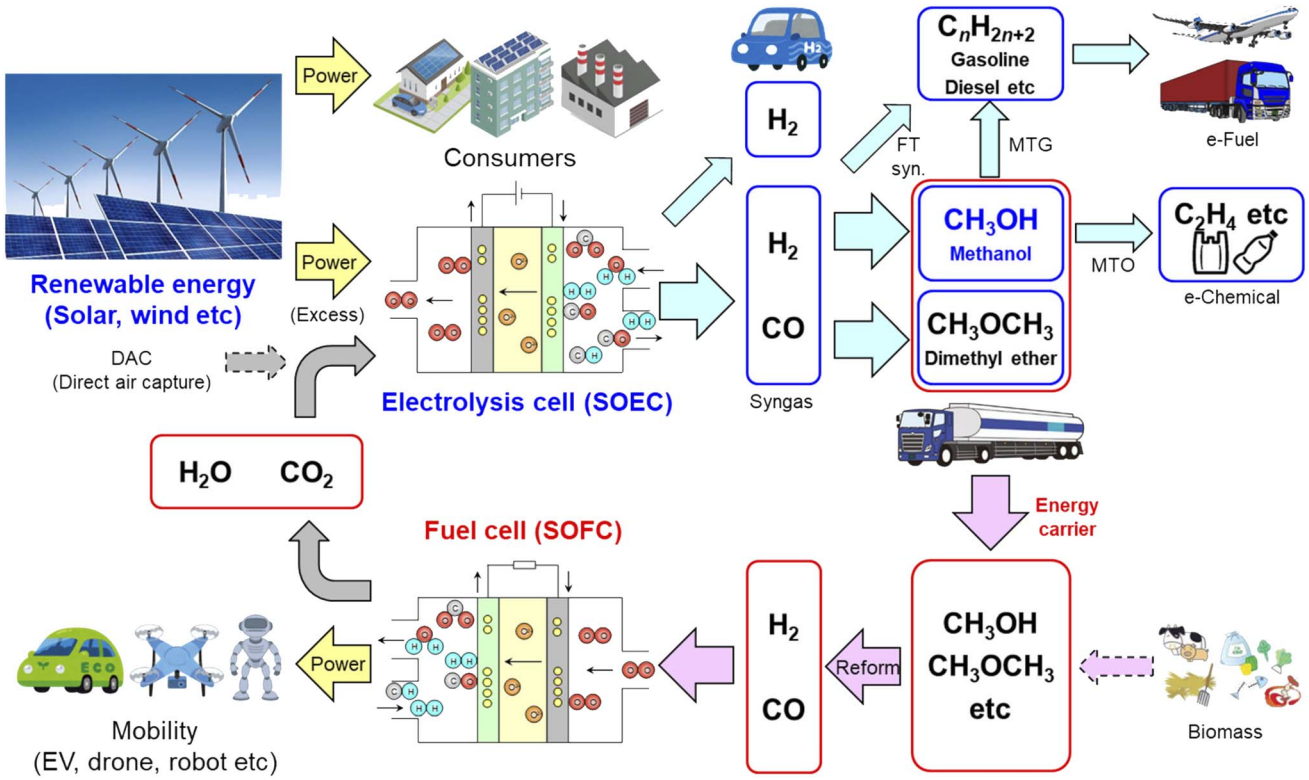

Fig. 16 Schematic of carbon-neutral energy system using co-electrolysis SOECs and internal reforming SOFCs.

power are supplied to consumers such as houses, buildings, and plants. The excess electric power is converted into chemical energy. Hydrogen is produced using SOECs in addition to alkaline and PEM electrolysis, and can be used in stationary fuel cells and fuel cell vehicles.[7] Syngas is also produced using SOECs, and converted into MeOH and DME.[20–22,28] Synthetic gasoline, kerosene, and diesel (e-fuel) are produced from syngas *via* FT synthesis, and can be used for airplanes, vessels, and large vehicles.[18,19] Methanol can be converted into gasoline (MTG; methanol to gasoline), olefin (MTO; methanol to olefins) such as ethylene and propylene, and aromatics (MTA; methanol to aromatics) such as benzene, toluene, and xylene. MTO widely contributes to carbon-neutral manufacturing processes for commodity plastics (e-chemical), whereas the raw materials of engineering plastics such as polycarbonate and polyurethane are directly synthesized from CO_2.[41] MeOH is a liquid at ordinary temperatures and pressures, and DME is easily liquified at 0.6 MPa. Therefore, MeOH and DME are promising energy carriers and fuels for internal reforming SOFCs. Biomass is also used as a fuel in SOFCs after desulfurization and reforming. Although CO_2 is exhausted from internal reforming SOFCs, it can be used for co-electrolysis SOECs. Mass and heat balance should be considered to achieve carbon neutrality. Thus, co-

electrolysis SOECs and internal reforming SOFCs significantly contribute to achieving a carbon-neutral society.

4. Conclusion

In the present work, H_2O/CO_2 co-electrolysis SOECs and internal reforming SOFCs using MeOH and DME were investigated using negatrode-supported microtubular cells with the same cell configuration. The co-electrolysis performance decreased with increasing CO_2 concentration in the input gas owing to an increase in polarization resistance related to gas diffusion process at the negatrode. The diffusion of CO/CO_2 mixture was more difficult than that of H_2/H_2O mixture in the SOEC negatrode. The gas diffusion resistance increased with time during co-electrolysis SOECs at $H_2O/CO_2 = 2$ and 700 °C. At various H_2O/CO_2 ratios, the faradaic efficiencies exceeded 96%, and the H_2/CO ratios of the product gases were almost identical to the H_2O/CO_2 ratios of the input gases. During the durability test at $H_2O/CO_2 = 2$, the faradaic efficiency and H_2/CO ratio of the product gas were stable for 100 h.

MeOH and DME can be produced industrially from syngas with an H_2/CO ratio of 2. The *I–V* characteristics were similar during internal reforming of MeOH and DME. The polarization resistances related to charge transfer and gas diffusion processes increased with time during internal reforming of MeOH and DME. Thus, the gas diffusion resistance should be decreased to improve the initial performance and durability of co-electrolysis SOECs and internal reforming SOFCs. In thermodynamic equilibrium, carbon is deposited at S/C <0.3 for MeOH, and at S/C <0.8 and O/C <0.9 for DME during steam and partial oxidation reforming, respectively. The internal reforming SOFCs successfully operated for 100 h at S/C ≥0.5 for MeOH, S/C ≥1.0 and O/C ≥1.0 for DME. Therefore, MeOH and DME syntheses from syngas *via* co-electrolysis SOECs and power generation *via* internal reforming SOFCs using MeOH and DME will contribute to achieving a carbon-neutral society.

Author contributions

Hirofumi Sumi: conceptualization, methodology, resources, data curation, investigation, writing – original draft preparation.

Conflicts of interest

There are no conflicts to declare.

References

1 K. Eguchi, H. Kojo, T. Takeguchi, R. Kikuchi and K. Sasaki, Fuel Flexibility in Power Generation by Solid Oxide Fuel Cells, *Solid State Ionics*, 2002, **152–153**, 411–416.
2 H. Sumi, K. Ukai, Y. Mizutani, H. Mori, C.-J. Wen, H. Takahashi and O. Yamamoto, Performance of Nickel-Scandia-Stabilized Zirconia Cermet Anodes for SOFCs in 3% H_2O-CH_4, *Solid State Ionics*, 2004, **174**, 151–156.
3 H. Sumi, T. Yamaguchi, K. Hamamoto, T. Suzuki and Y. Fujishiro, Impact of Direct Butane Microtubular Solid Oxide Fuel Cells, *J. Power Sources*, 2012, **220**, 74–78.
4 H. Sumi, T. Yamaguchi, H. Shimada, Y. Fujishiro and M. Awano, Internal Partial Oxidation Reforming of Butane and Steam Reforming of Ethanol for Anode-supported Microtubular Solid Oxide Fuel Cells, *Fuel Cells*, 2017, **17**, 875–881.
5 H. Sumi, S. Nakabayashi, T. Kawada, Y. Uchiyama, N. Uchiyama and K. Ichihara, Demonstration of SOFC Power Sources for Drones (UAVs; Unmanned Aerial Vehicles), *ECS Trans.*, 2019, **91**(1), 149–157.
6 Y. Shiratori, T. Ijichi, T. Oshima and K. Sasaki, Internal Reforming SOFC Running on Biogas, *Int. J. Hydrogen Energy*, 2010, **35**, 7905–7912.
7 S. A. Grigoriev, V. N. Fateev, D. G. Bessarabov and P. Millet, Current Status, Research Trends, and Challenges in Water Electrolysis Science and Technology, *Int. J. Hydrogen Energy*, 2020, **45**, 26036–26058.
8 R. Küngas, Review-Electrochemical CO_2 Reduction for CO Production: Comparison of Low- and High-temperature Electrolysis Technologies, *J. Electrochem. Soc.*, 2020, **167**, 044508.
9 A. A. Olajire, CO_2 Capture and Separation Technologies for End-of-pipe Applications - A Review, *Energy*, 2010, **35**, 2610–2628.
10 F. Bisotti, K. A. Hoff, A. Mathisen and J. Hovland, Direct Air capture (DAC) Deployment: A Review of the Industrial Deployment, *Chem. Eng. Sci.*, 2024, **283**, 119416.
11 Y. Kohno, M. Kanakubo, M. Iwaya, Y. Yamato and T. Makino, Ionic Liquid Mixtures for Direct Air Capture: High CO_2 Permeation Driven by Superior CO_2 Absorption with Lower Absolute Enthalpy, *ACS Omega*, 2022, **7**, 42155–42162.
12 C. Graves, S. D. Ebbesen and M. Mogensen, Co-electrolysis of CO_2 and H_2O in Solid Oxide Cells: Performance and Durability, *Solid State Ionics*, 2011, **192**, 398–403.
13 S. D. Ebbesen, R. Knibbe and M. Mogensen, Co-electrolysis of Steam and Carbon Dioxide in Solid Oxide Cells, *J. Electrochem. Soc.*, 2012, **159**, F482–F489.
14 D. M. A. Duenas, M. Riedel, M. Riegraf, R. Costa and K. A. Friedrich, High Temperature Co-electrolysis for Power-to-X, *Chem. Ing. Tech.*, 2020, **92**, 45–52.
15 C. Xi, J. Sang, A. Wu, J. Yang, X. Qi, W. Guan, J. Wang and S. C. Singhal, Electrochemical Performance and Durability of Flat-tube Solid Oxide Electrolysis Cells for H_2O/CO_2 Co-electrolysis, *J. Catal.*, 2021, **404**, 174–186.
16 E. Ioannidou, M. Chavani, S. G. Neophytides and D. K. Niakolas, Effect of the P_{H2O}/P_{CO2} and P_{H2} on the Intrinsic Electro-catalytic Interactions and the CO Production Pathway on Ni/GDC during Solid Oxide H_2O/CO_2 Co-electrolysis, *Int. J. Hydrogen Energy*, 2022, **47**, 10166–10174.
17 C. Mebrahtu, M. Nohl, L. Dittrich, S. R. Foit, L. G. J. de Haart, R.-A. Eichel and R. Palkovits, Integrated Co-Electrolysis and Syngas Methanation for the Direct Production of Synthetic Natural Gas from CO_2 and H_2O, *ChemSusChem*, 2021, **14**, 2295–2302.

18 M. E. Dry, The Fischer-Tropsch Process: 1950-2000, *Catal. Today*, 2002, **71**, 227–241.
19 N. Koizumi, T. Mochizuki and M. Yamada, Preparation of Highly Active Catalysts for Ultra-clean Fuels, *Catal. Today*, 2009, **141**, 34–42.
20 G. Bozzano and F. Manenti, Efficient Methanol Synthesis: Perspectives, Technologies and Optimization Strategies, *Prog. Energy Combust. Sci.*, 2016, **56**, 71–105.
21 S. Mbatha, R. C. Everson, N. M. Musyoka, H. W. Langmi, A. Lanzini and W. Brilman, Power-to-methanol Process: A review of Electrolysis, Methanol Catalysts, Kinetics, Reactor Designs and Modelling, Process Integration, Optimisation, and Techno-economics, *Sustain. Energy Fuels*, 2021, **5**, 3490–3569.
22 Y. Choi, K. Futagami, T. Fujitani and J. Nakamura, The Difference in the Active Sites for CO_2 and CO Hydrogenations on Cu/ZnO-based Methanol Synthesis Catalysts, *Catal. Lett.*, 2001, **73**, 27–31.
23 A. S. Arico, S. Srinivasan and V. Antonucci, DMFCs: From Fundamental Aspects to Technology Development, *Fuel Cells*, 2001, **1**, 133–161.
24 T. Kim, K. Ahn, J. M. Vohs and R. J. Gorte, Deactivation of Ceria-based SOFC Anodes in Methanol, *J. Power Sources*, 2007, **164**, 42–48.
25 M. Liu, R. Peng, D. Dong, J. Gao, X. Liu and G. Meng, Direct Liquid Methanol-fueled Solid Oxide Fuel Cell, *J. Power Sources*, 2008, **185**, 188–192.
26 M. Lo Faro, A. Stassi, V. Antonucci, V. Modafferi, P. Frontera, P. Antonucci and A. S. Aricò, Direct Utilization of Methanol in Solid Oxide Fuel Cells: An Electrochemical and Catalytic Study, *Int. J. Hydrogen Energy*, 2011, **36**, 9977–9986.
27 Z. Gao, R. Raza, B. Zhu and Z. Mao, Development of Methanol-fueled Low-temperature Solid Oxide Fuel Cells, *Int. J. Energy Res.*, 2011, **35**, 690–696.
28 K. Omata, Y. Watanabe, T. Umegaki, G. Ishiguro and M. Yamada, Low-pressure DME Synthesis with Cu-based Hybrid Catalysts using Temperature-gradient Reactor, *Fuel*, 2002, **81**, 1605–1609.
29 S. Wang, T. Ishihara and Y. Takita, Dimethyl Ether Fueled Intermediate Temperature SOFC Using $LaGaO_3$-Based Perovskite Electrolytes, *Electrochem. Solid-State Lett.*, 2002, **5**, A177–A180.
30 C. Su, W. Wang, H. Shi, R. Ran, H. J. Park, C. Kwak and Z. Shao, Reducing the Operation Temperature of a Solid Oxide Fuel Cell Using a Conventional Nickel-based Cermet Anode on Dimethyl Ether Fuel through Internal Partial Oxidation, *J. Power Sources*, 2011, **196**, 7601–7608.
31 M. A. Laguna-Bercero, Recent Advances in High Temperature Electrolysis using Solid Oxide Fuel Cells: A Review, *J. Power Sources*, 2012, **203**, 4–16.
32 K. Hosoi, H. Hagiwara, S. Ida and T. Ishihara, $La_{0.8}Sr_{0.2}FeO_{3-\delta}$ as Fuel Electrode for Solid Oxide Reversible Cells Using $LaGaO_3$-Based Oxide Electrolyte, *J. Phys. Chem. C*, 2016, **120**, 16110–16117.
33 H. Uchida, H. Nishino, P. Puengjinda and K. Kakinuma, Remarkably Improved Durability of Ni-Co Dispersed Samaria-Doped Ceria Hydrogen Electrodes by Reversible Cycling Operation of Solid Oxide Cells, *J. Electrochem. Soc.*, 2020, **167**, 134516.
34 H. Schichlein, A. C. Muller, M. Voigts, A. Krugel and E. Ivers-Tiffée, Deconvolution of Electrochemical Impedance Spectra for the Identification of Electrode Reaction Mechanisms in Solid Oxide Fuel Cells, *J. Appl. Electrochem.*, 2002, **32**, 875–882.
35 A. Leonide, B. Rüger, A. Weber, W. A. Meulenberg and E. Ivers-Tiffée, Evaluation and Modeling of the Cell Resistance in Anode-supported Solid Oxide Fuel Cells, *J. Electrochem. Soc.*, 2010, **157**, B234–B239.
36 H. Sumi, H. Shimada, Y. Yamaguchi, T. Yamaguchi and Y. Fujishiro, Degradation Evaluation by Distribution of Relaxation Times Analysis for Microtubular Solid Oxide Fuel Cells, *Electrochim. Acta*, 2020, **339**, 135913.
37 J. Weese, A Reliable and Fast Method for the Solution of Fredhol Integral Equations of the First Kind Based on Tikhonov Regularization, *Comput. Phys. Commun.*, 1992, **69**, 99–111.
38 E. Ivers-Tiffée and A. Weber, Evaluation of Electrochemical Impedance Spectra by the Distribution of Relaxation Times, *J. Ceram. Soc. Jpn.*, 2017, **125**, 193–201.
39 B. A. Boukamp, A Linear Kronig-Kramers Transform Test for Immittance Data Validation, *J. Electrochem. Soc.*, 1995, **142**, 1885–1894.
40 M. Schönleber, D. Klotz and E. Ivers-Tiffée, A Method for Improving the Robustness of Linear Kramers-Kronig Validity Tests, *Electrochim. Acta*, 2014, **131**, 20–27.
41 W. S. Putro, A. Ikeda, S. Shigeyasu, S. Hamura, S. Matsumoto, V. Y. Lee, J.-C. Choi and N. Fukaya, Sustainable Catalytic Synthesis of Diethyl Carbonate, *ChemSusChem*, 2021, **14**, 842–846.